Molecular Catalysis 444 (2018) 10–21

Contents lists available at ScienceDirect

Molecular Catalysis

journal homepage: www.elsevier.com/locate/mcat

Editor's choice paper

MoO_3 supported on ordered mesoporous zirconium oxophosphate: An efficient and reusability solid acid catalyst for alkylation and esterification

Zhichao Miao, Zhenbin Li, Jinping Zhao, Weijiang Si, Jin Zhou*, Shuping Zhuo*

School of Chemistry and Chemical Engineering, Shandong University of Technology, Zibo, 255049, PR China

ARTICLE INFO

Article history:
Received 11 July 2017
Received in revised form
13 September 2017
Accepted 23 October 2017

Keywords:
Mesoporous solid acid
MoO_3 loadings
Calcination temperature
FC alkylation
Esterification

ABSTRACT

A series of molybdenum oxide supported on ordered mesoporous zirconium oxophosphate (MoO_3/M-ZrPO) materials with different MoO_3 loadings (0–20 wt%) and calcination temperatures (500–900 °C) have been designed, synthesized and employed as solid acid catalysts in alkylation and esterification. The XRD, TG-DSC, H_2-TPR, N_2-physisorption and TEM characterizations were taken to investigate the structural properties and states of introduced MoO_3 species. The influence of MoO_3 loadings and calcination temperatures in catalytic performance was detailedly investigated and optimal catalytic activity was reached at 10 wt% MoO_3 loadings and treated at 700 °C. Moreover, MoO_3/M-ZrPO catalysts exhibited outstanding catalytic performance in Friedel-Crafts alkylation of different aromatic compounds and esterification of levulinic acid with 1-butanol. Furthermore, it was noteworthy that the catalyst had superior reusability and no noticeable declines were observed in catalytic performance even after seven runs.

1. Introduction

As the backbone of petroleum and chemical processing industries, different kinds of acid-catalyzed reactions, such as isomerization [1,2], alkylation [3], dehydration [4,5] and esterification [6], are widely investigated. However, use of cheap and available homogeneous acid catalysts (e.g. $AlCl_3$, $FeCl_3$, HCl and H_2SO_4) has led to severe environmental problems [7,8]. Therefore, continuous efforts have been taken to replace these conventional catalysts with solid acid catalysts, which are easy separation, little corrosion, environmentally friendly and little pollution and waste [9,10]. As a new generation of solid acid catalyst, Zr-based solid acid catalysts (e.g. WO_3/ZrO_2 [11,12], MoO_3/ZrO_2 [13,14] and B_2O_3/ZrO_2 [15]), which have strong acidic properties and high stability, have attracted considerable attention since their initial discovery in the late 1980s. In addition, as reported by other workers, there exist different influence factors, such as loadings of modifiers (W, Mo and B), calcination temperatures and crystalline phase of ZrO_2 on catalytic performance [16–19]. Therefore, it is important to investigate these factors systematically to get an excellent solid acid catalyst.

Friedel-Crafts (FC) alkylation of aromatic compounds is one of the most important strategies to synthesis a wide variety of diarylalkanes in organic chemistry, which have significant commercial value and key intermediates in the fields of petrochemicals, pharmaceuticals, cosmetics, dyes and many other important chemical industries [20–23]. Furthermore, as for alkylating agents, benzyl alcohol, which only products H_2O as byproduct is more preferable than others [21,24,25]. Traditionally, strong Lewis acid catalysts ($AlCl_3$, $FeCl_3$ and BF_3) and Brønsted acid catalysts (H_2SO_4, HCl and HNO_3) are employed in FC alkylation [26]. These years, different solid acid catalysts which are environmentally friendly, such as magnetic carbon [27], TiO_2 nanosheets [28], zeolites [29] and MOFs [30], are employed and investigated in FC alkylation reactions.

Esterification reaction is a significant reaction for production of fuels and chemicals [31,32]. Levulinic acid esters, which can be synthesized by esterification of levulinic acid (LA) with 1-butanol, have drawn plentiful attentions owing to the potential applications in domains of fuel additives, green solvents, fragrances, lubricants and polymer productions [33–35]. More important, LA can be gotten from hydrolysis of renewable cellulosic materials and it is an alternative renewable energy resource. These years, various solid acid catalysts were utilized for esterification of LA including WO_3-SBA-16 [36], WO_x/ZrO_2 [37] and heteropolyacids [38].

In comparison of traditional bulk materials, ordered mesoporous materials have attracted a lot of attentions, because of their outstanding textural properties such as large accessible surface

* Corresponding author.
E-mail addresses: zhoujin@sdut.edu.cn (J. Zhou), zhuosp_academic@yahoo.com (S. Zhuo).

http://dx.doi.org/10.1016/j.mcat.2017.10.028
2468-8231/

area, big pore size and volume [39–42]. As for supported catalysts, mesoporous materials are promising supports for improving the dispersion of active component to provide abundant active sites for reactant molecules. This might be in favor of the enhancement of catalytic performance [43–45]. Therefore, mesoporous materials have potential to be investigated in the field of support.

In this work, we focus on synthesizing a sequence of MoO_3 supported on the ordered mesoporous zirconium oxophosphate (M-ZrPO) with various MoO_3 loadings and taken as solid acid catalyst for FC alkylation of different aromatic compounds and esterification of levulinic acid with 1-butanol. The aim of this work is to investigate the influence of MoO_3 loadings and calcination temperatures on catalytic performance and get an excellent solid acid catalyst. In addition, the MoO_3/M-ZrPO materials were detailedly characterized by N_2-physisorption, TEM, XRD and H_2-TPR characterizations for mesoporous properties and states of Mo species in the materials. Moreover, the possible structure-function relationship was discussed and the influences of MoO_3 loadings and calcination temperatures on catalytic performance were detailedly investigated.

2. Experimental section

2.1. Catalyst preparation

Ordered mesoporous zirconium oxophosphate (M-ZrPO) was prepared as reported in the previous report [46]. The supported MoO_3 solid acid catalysts were synthesized through the equivalent-volume impregnation method with ammonium molybdate ($(NH_4)_6Mo_7O_{24}{\cdot}4H_2O$) aqueous solution as precursor of MoO_3. After the process of impregnation, the materials were treated at 120 °C for 12 h and calcined at 700 °C for 4 h. The synthesized catalysts were named as X wt% MoO_3/M-ZrPO and X wt% ($X\,wt\% = m_{MoO3}/(m_{MoO3} + m_{M\text{-}ZrPO}) \times 100\%$) stood for the loadings of MoO_3. The 10 wt% MoO_3/M-ZrPO catalysts treated at different temperatures were denotes as 10 wt% MoO_3/M-ZrPO-Y and Y stood for calcination temperatures (500, 600, 700, 800 and 900 °C).

2.2. Characterization

X-ray diffraction (XRD) patterns were recorded on an X'Pert Pro Multipurpose diffractometer (Bruker AXS D8 Advance) with Cu Kα radiation (0.15406 nm) at room temperature from 10.0° to 80.0° (voltage 40 kV, current setting 20 mA, step size 0.02°, count time 4 s).

Thermogravimetric-differential scanning calorimetry (TG-DSC) characterizations were taken on a NETZSCH STA 449C thermogravimetric analyzer from room temperature to 1000 °C with the rate of 10 °C min^{-1} under air atmosphere.

H_2 temperature-programmed reduction (H_2-TPR) measurements were performed on a Chembet PULSAR TPR/TPD (Quantachrome Instruments U.S.). The sample (0.1 g) was loaded in a U-shaped quartz reactor. Prior to the test, sample was pretreated at 500 °C for 1 h in flowing He gas (40 mL min^{-1}) to remove any moisture and other adsorbed impurities. After cooling the reactor to 40 °C, a 5% H_2-Ar gas (40 mL min^{-1}) mixture was introduced. The catalyst was heated to 1000 °C at a rate of 20 °C min^{-1} and the H_2 gas consumption was measured using a TCD detector.

The nitrogen adsorption and desorption isotherms at −196 °C were recorded on a Micromeritics ASAP 2020 static volumetric analyzer. Prior to the test, the sample was pretreated at 200 °C for 2 h. The specific surface areas were calculated via the Brunauer-Emmett-Teller (BET) method in the relative pressure range of 0.05-0.3; the single-point pore volume was calculated from the adsorption isotherm at a relative pressure of 0.990; pore size distributions were calculated using adsorption branches of nitrogen adsorption-desorption isotherms by Barrett-Joyner-Halenda (BJH) method.

Transmission electron microscopy (TEM) images and elemental mapping measurements were carried out on TECNAI G^2 F20 high-resolution transmission electron microscopy under a working voltage of 200 kV.

Temperature programmed desorption of ammonia (NH_3-TPD) was performed on a Finesorb 3010 (FINETEC INSTRUMENTS). The typical experiment for TPD measurement was carried out as follows: prior to the test, the sample (0.1 g) was pretreated at 500 °C for 1 h under the flowing He to remove the moisture and absorbed impurities. After cooling to 100 °C, NH_3-He (0.5-99.5 mol%) was introduced for 30 min. The physically absorbed NH_3 in the sample was removed by blowing in He at 100 °C for 60 min. Afterwards, the TPD experiment was carried out by increasing the temperature to 500 °C at a rate of 10 °C min^{-1} and the desorbed NH_3 was measured by TCD detector.

The infrared spectra of adsorbed pyridine (Pyridine-IR spectra) were taken on PE Frontier FT-IR spectrometer. Prior to the test, the sample was pretreated at 400 °C for 1 h under 5×10^{-3} Pa, afterwards, the sample was cooled to room temperature and pyridine was introduced. Then, the sample was raised to 200 °C and held for 30 min under 5×10^{-3} Pa, after which the spectrum was recorded. The blank experiments were operated under the same conditions and employed as the background to insure the accuracy of the infrared spectra of adsorbed pyridine.

X-ray fluorescence (XRF) spectra were recored on a ZSX-100e (Rigaku Corporation).

2.3. Catalytic reaction

The liquid phase Friedel-Crafts (FC) alkylation with different aromatic compounds and alkylating agents was taken in round bottom flask accompanied with a reflux condenser in a temperature controlled oil bath. In a typical run for alkylation of anisole with benzyl alcohol, anisole (10 mL), benzyl alcohol (1 mL) and catalysts (0.1 g) were successively added into a round bottom flask. Then, the reaction was performed under reflux condition and magnetic stirring for 1 h. The used catalysts were separated and treated at 500 °C for 1 h and employed in next cycle. The conversion of reactants and selectivity of products were detected by a gas chromatography (GC) instrument (Agilent-7890B; equipped with a flame ionization detector (FID) and PE-6 column (50 m × 0.32 mm × 0.25 μm)). The qualitative analysis of reaction products was confirmed by gas chromatography-mass spectroscopy (GC-MS) (GCMS-QP2010 SE, SHIMADZU). The *o*-benzylanisoles (*o*-BA), *p*-benzylanisoles (*p*-BA) and dibenzyl ether (DBE) were detected and no other products were observed in this reaction. The conversion of benzyl alcohol ($X_{benzylalcohol}$) and selectivity of BA (S_{BA}) were calculated according to the following equations:

$$X_{benzyl\ alcohol}(\text{mol\%}) = \frac{\text{mole of benzyl alcohol reacted}}{\text{mole of benzyl alcohol initially}} \times 100\ \text{mol\%}$$

$$S_{BA}(\text{mol\%}) = \frac{o\text{-BA} + p\text{-BA}}{o\text{-BA} + p\text{-BA} + \text{DBE}} \times 100\ \text{mol\%}$$

Moreover, esterification of levulinic acid (LA) with 1-butanol was performed and analyzed as aforementioned method. In a typical run, 0.1 g of catalyst was added to a mixture (1-butanol (10 mL) + LA (1 mL)). The reaction was carried out at 120 °C for 4 h. The conversion of LA and selectivity of products were detected as above-mentioned GC instrument. The *normal*-butyl levulinate (*n*-BL) and *pseudo*-butyl levulinate (*p*-BL) were detected and no other products were observed in this reaction. The conversion of

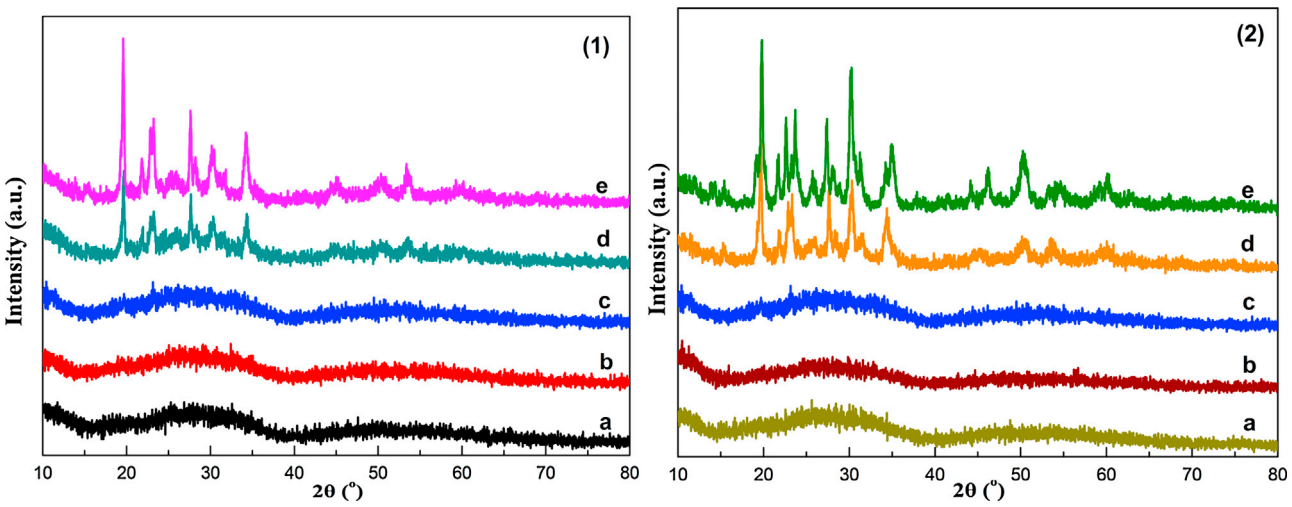

Fig 1. X-ray diffraction patterns: **(1)** MoO_3/M-ZrPO with differernt MoO_3 loadings treated at 700 °C: **(a)** 0 wt% MoO_3/M-ZrPO, **(b)** 5 wt% MoO_3/M-ZrPO, **(c)** 10 wt% MoO_3/M-ZrPO, **(d)** 15 wt% MoO_3/M-ZrPO, **(e)** 20 wt% MoO_3/M-ZrPO; **(2)** 10 wt% MoO_3/M-ZrPO treated at different temperatures: **(a)** 500 °C, **(b)** 600 °C, **(c)** 700 °C, **(d)** 800 °C, **(e)** 900 °C.

LA (X_{LA}) and selectivity of *n*-BL ($S_{n\text{-}BL}$) were calculated according to the following equations:

$$X_{LA}(\text{mol\%}) = \frac{\text{mole of LA reacted}}{\text{mole of LA initially}} \times 100\ \text{mol\%}$$

$$S_{n-BL}(\text{mol\%}) = \frac{n\text{-BL}}{n\text{-BL} + p\text{-BL}} \times 100\ \text{mol\%}$$

3. Results and discussion

3.1. XRD analysis

XRD characterization is taken to investigate the crystalline structure of materials. The patterns of MoO_3/M-ZrPO solid acid catalysts with different MoO_3 loadings are depicted in Fig. 1(1). The sample without introducing MoO_3 species, only presented two broad peaks, showing the existence of amorphous structure without crystalline structure in M-ZrPO support. Moreover, materials with MoO_3 loadings under 10 wt% exhibited similar profile to M-ZrPO. The lack of exclusive crystalline MoO_3 peaks showed that introduced Mo species had a highly dispersed state on the M-ZrPO surface or the MoO_3 clusters were too small to be confirmed by XRD characterization in these samples. However, with MoO_3 loadings increasing to 15 and 20 wt%, observable diffraction peaks appeared, implying that some of introduced Mo species assembled on the M-ZrPO and turned into crystalline MoO_3 (JCPDF No. 05-0508). In addition, with the formation of crystalline MoO_3, amorphous structure of M-ZrPO was destroyed and transformed to crystalline $Zr_2O(PO_4)_3$ (JCPDF No. 37-0155) structure (Fig. S1(1)).

XRD patterns of 10 wt% MoO_3/M-ZrPO calcined at different temperatures are provided in Fig. 1(2). The highly dispersed Mo species existed in samples treating at 500, 600 and 700 °C. Afterwards, further increasing calcination temperature to 800 and 900 °C, Mo species aggregated and crystalline structure appeared. The same conclusion also could be confirmed by TG-DSC technology of as-synthesized 10 wt% MoO_3/M-ZrPO. As displayed in Fig. 2, a weigh loss and endothermic peak under 400 °C was attributed to the decomposition of precursors. In addition, the absence of obvious weight loss at 500–700 °C implied that precursors completely decomposed and formed MoO_3 species. The small weight loss with an exothermic peak at about 750 °C was ascribed to the pore wall transformation from amorphous to crystalline structure. Compared

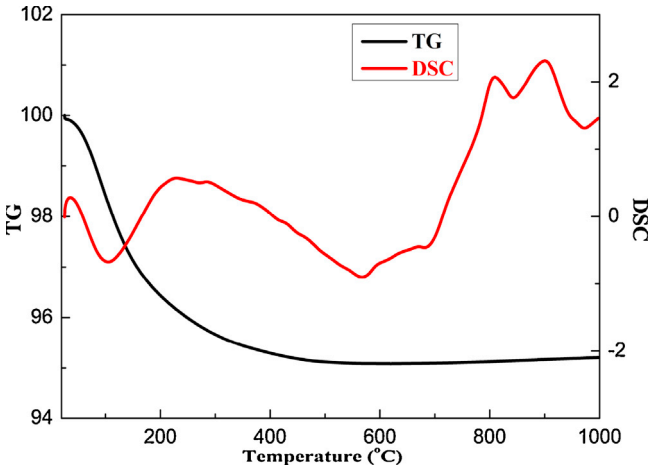

Fig. 2. TG-DSC curves of the as-synthesized 10 wt% MoO_3/M-ZrPO.

with this, amorphous structure could exist even treated at 800 °C for M-ZrPO support (Fig. S1(2)). This might be owing to that introducing Mo species began to form crystalline aggregations at high MoO_3 loadings and calcination temperature and induced transformation of amorphous structure to crystalline structure for M-ZrPO support.

3.2. H_2-TPR analysis

H_2-TPR patterns are taken to analyse existing states of introduced Mo species. As displayed in Fig. 3(1), the H_2-TPR profiles of MoO_3/M-ZrPO solid acid catalysts with different MoO_3 loadings exhibited different patterns. For the sample without introducing Mo species, there exhibited no obvious peak in 300–1000 °C, showing no reducible species existed on M-ZrPO. With introducing of Mo species, reduction peak could be observed at about 450 °C in pattern of 5 wt% MoO_3/M-ZrPO, which was attributed to the reduction of dispersed polymolybdate species [47–49]. Further increasing the MoO_3 loadings to 10 wt%, a new reduction peak, which was ascribed to the reduction of crystalline MoO_3 species, could be observed at about 900 °C [47]. However, no obvious diffraction peaks owing to crystalline MoO_3 species were discovered in XRD pattern of 10 wt% MoO_3/M-ZrPO. This might be owing to that the size of crystalline MoO_3 species was too small to be confirmed by XRD technology.

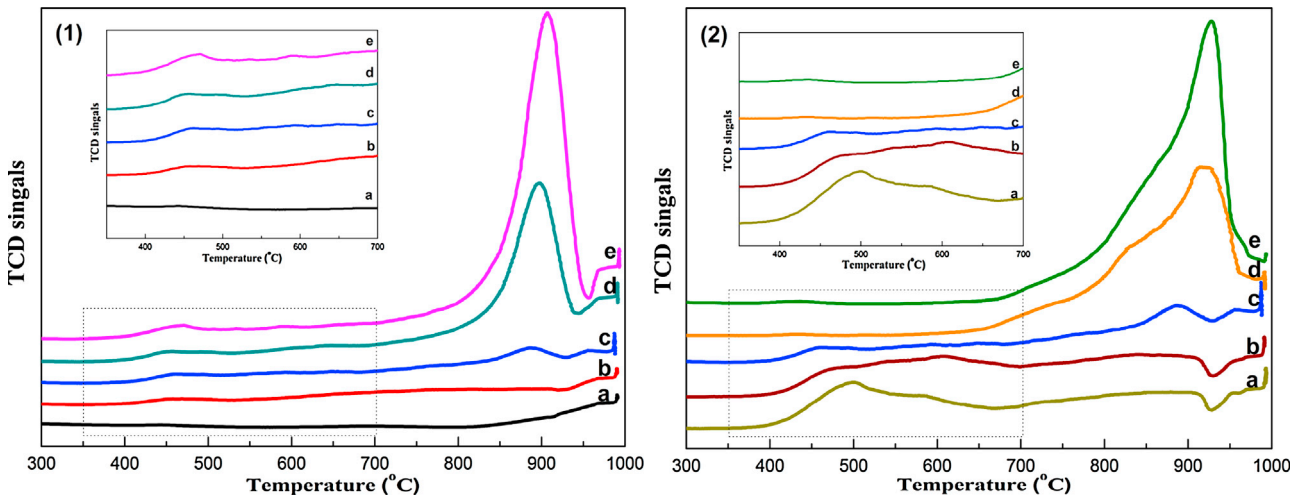

Fig. 3. The H_2-TPR profiles: **(1)** MoO_3/M-ZrPO with differernt MoO_3 loadings treated at 700 °C: **(a)** 0 wt% MoO_3/M-ZrPO, **(b)** 5 wt% MoO_3/M-ZrPO, **(c)** 10 wt% MoO_3/M-ZrPO, **(d)** 15 wt% MoO_3/M-ZrPO, **(e)** 20 wt% MoO_3/M-ZrPO; **(2)** 10 wt% MoO_3/M-ZrPO treated at different temperatures: **(a)** 500 °C, **(b)** 600 °C, **(c)** 700 °C, **(d)** 800 °C, **(e)** 900 °C.

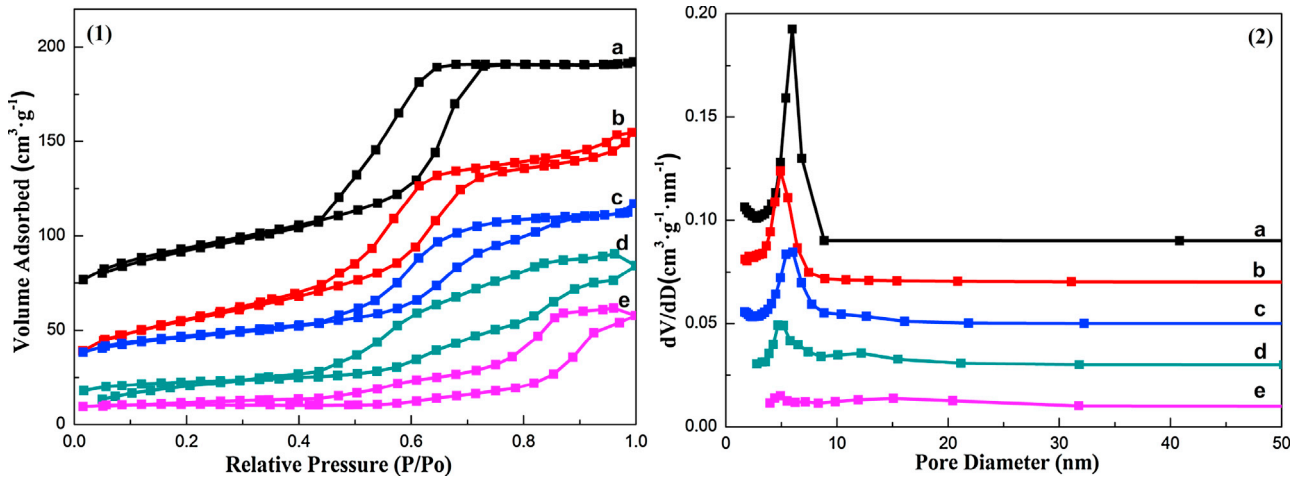

Fig. 4. Isotherm **(1)** and pore size distributions **(2)** of MoO_3/M-ZrPO with differernt MoO_3 loadings treated at 700 °C: **(a)** 0 wt% MoO_3/M-ZrPO, **(b)** 5 wt% MoO_3/M-ZrPO, **(c)** 10 wt% MoO_3/M-ZrPO, **(d)** 15 wt% MoO_3/M-ZrPO, **(e)** 20 wt% MoO_3/M-ZrPO.

As for 15 wt% MoO_3/M-ZrPO and 20 wt% MoO_3/M-ZrPO samples, obvious peaks could be found at about 900 °C, showing Mo species mainly existed as crystalline MoO_3 phase in samples, further confirming the XRD analysis, which displayed obvious diffraction peaks for crystalline MoO_3 species.

H_2-TPR profiles of 10 wt% MoO_3/M-ZrPO solid acid catalysts with different calcination temperatures are displayed in Fig. 3(2). Although these samples had same MoO_3 loadings, they exhibited entirely different profiles. Specifically, as for the materials treated at 500 and 600 °C, reduction peaks only appeared at 400–700 °C, showing the existence of dispersed polymolybdates in the samples. With the increasing of calcination temperatures, intensity of peaks at 400–700 °C became weaker and vanished in 10 wt% MoO_3/M-ZrPO-800 and 10 wt% MoO_3/M-ZrPO-900 samples. Meanwhile, the peaks at 800–950 °C appeared, indicating the highly dispersed polymolybdates transformed to crystalline MoO_3 species at high calcination temperature, further confirming the aforementioned XRD characterizations.

3.3. Nitrogen adsorption-desorption analysis

The textural properties and Mo atom density of MoO_3/M-ZrPO samples are investigated by nitrogen adsorption-desorption isotherms. As shown in Fig. 4(1), samples with MoO_3 loadings under 10 wt%, presented typical IV type isotherm with H1 shaped hysteresis loops observed in the P/P_0 range from 0.4 to 0.7. With MoO_3 loadings increasing to 15 and 20 wt%, the isotherms began to deform and hysteresis loop changed to the type between H1 and H2, indicating existence of cage-like mesopores or cylindrical mesopores with partial distortion. This might be owing to the formation of crystalline MoO_3 particles led to the transformation of amorphous skeleton to crystalline structure and the ordered mesoporous structure of M-ZrPO was destoryed. In addition, as presented in Fig. 4(2), the samples with MoO_3 loadings under 10 wt% showed obvious distribution around 5 nm, proving the successful preservation of ordered mesostructure. Moreover, for 15 wt% MoO_3/M-ZrPO and 20 wt% MoO_3/M-ZrPO samples, absence of obvious pore size distributions indicated the disappearance of ordered mesoporous structure in materials.

Nitrogen adsorption-desorption isotherms and pore size distributions of 10 wt% MoO_3/M-ZrPO treated at different temperatures are given in Fig. 5. For samples with calcination temperature below 700 °C, ordered mesostructure with uniform pore size distribution were observed. However, with the temperature increasing to 800 and 900 °C, mesoporous structure vanished and no obvious pore

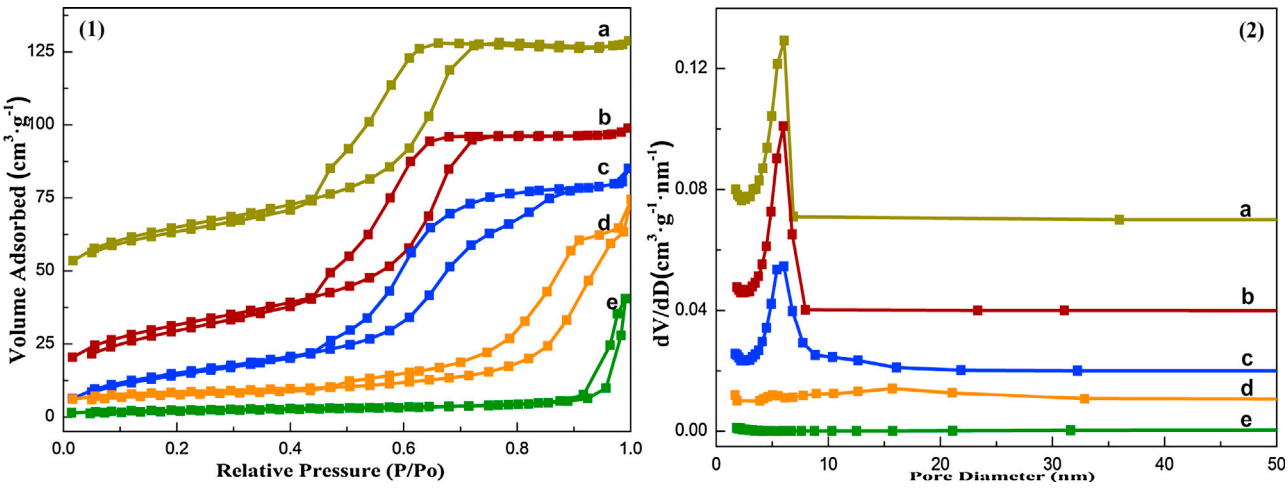

Fig. 5. Isotherm **(1)** and pore size distributions **(2)** of 10 wt% MoO_3/M-ZrPO treated at different temperatures: **(a)** 500 °C, **(b)** 600 °C, **(c)** 700 °C, **(d)** 800 °C, **(e)** 900 °C.

Table 1
Textural properties and acidity of the MoO_3/M-ZrPO samples.

Samples	Nitrogen physisorption			Mo atom density (atom nm^{-2})[a]	Total acidity (mmol/g)[b]
	Specific Surface Area ($m^2\ g^{-1}$)	Pore size (nm)	Pore Volume ($cm^3\ g^{-1}$)		
0 wt% MoO_3/M-ZrPO-700	121	5.61	0.19	0	0.103
5 wt% MoO_3/M-ZrPO-700	94	5.18	0.18	2.21	0.127
10 wt% MoO_3/M-ZrPO-700	82	6.62	0.15	5.11	0.148
15 wt% MoO_3/M-ZrPO-700	42	8.45	0.13	14.8	0.071
20 wt% MoO_3/M-ZrPO-700	16	13.4	0.09	51.5	0.035
10 wt% MoO_3/M-ZrPO-500	120	5.01	0.17	3.48	0.155
10 wt% MoO_3/M-ZrPO-600	111	5.81	0.17	3.77	0.144
10 wt% MoO_3/M-ZrPO-800	28	15.3	0.09	15.0	0.014
10 wt% MoO_3/M-ZrPO-900	8	–	0.05	51.6	0.008

[a] The Mo surface densities expressed as the number of Mo atoms per nanometer square area (Mo atoms nm^2) and were calculated using the equation: Surface density of Mo = {[MoO_3 loadings (wt%)/100] × 6.023 × 10^{23}}/{[144.0 (formula weight of MoO_3) × S_{BET} ($m^2\ g^1$) × 10^{18}]}.
[b] The acidity gotten from NH_3-TPD measurements.

size distributions were observed, implying the absence of ordered mesostructure at high calcination temperature.

The parameters of textural properties, such as specific surface area, pore size, pore volume and Mo atom density are given in Table 1. It could be clearly observed that textural properties of the samples sharply decreased with MoO_3 loadings up to 15 wt% and calcination temperature to 800 °C. Combined with XRD analyse, it could be summarized that MoO_3 species were highly dispersed on the surface of M-ZrPO when the Mo atom density was under 5.11 atom nm^{-2}. Moreover, crystalline MoO_3 began to form and ordered mesostructure was destroyed when the Mo atom density exceeded 14.8 atom nm^{-2}. This conclusion also could be demonstrated by the MoO_3/M-ZrPO with different MoO_3 loadings and treated at 600 °C (shown in Fig. S2, S3 and Table S1). When the MoO_3 loadings of samples were below 15 wt%, Mo atom density was under 6.45 atom nm^{-2} and Mo species existed as highly dispersed states. Further increasing the MoO_3 loadings up to 20 and 25 wt%, crystalline structure appeared and mesostructure was destroyed.

3.4. TEM analysis

The following TEM characterizations are constructed for purpose of illustrating the morphology of catalysts. As shown in Fig. 6a,b, obvious ordered mesoporous structure could be clearly observed with MoO_3 loadings under 10 wt%, implying ordered mesoporous structure existed and this further confirmed the characterization of N_2-physisorption, which predicted the presence of ordered mesostructure. Moreover, it was noteworthy that no obvious particles were found in these two samples, which had no obvious diffraction peaks in XRD patterns. With the increasing of MoO_3 loadings to 15 and 20 wt%, the mesostructure destroyed and obvious particles were observed. In order to give further consideration to the dispersion of introduced Mo species, elemental mapping of 10 wt% MoO_3/M-ZrPO was taken and shown in Fig. 7. It could be clearly observed that O, Zr, P and Mo elements were uniformly dispersed throughout the skeleton of material, showing that Mo species were introduced as designed and highly dispersed in the framework of M-ZrPO.

3.5. Acidic properties

The acidic properties of materials are evaluated by NH_3-TPD characterization. NH_3-TPD profiles of MoO_3/M-ZrPO solid acid catalysts with different MoO_3 loadings are given in Fig. 8(1). In these profiles, obvious peaks which caused by the desorption of NH_3 interacted with acid sites in the materials, could be clearly observed, implying the existence of abundant acid sites in the MoO_3/M-ZrPO materials. In addition, the intensity of peak and corresponding acidity (shown in Table 1) were enhanced with the MoO_3 loading increasing from 0 to 10 wt% and reached the maximum (0.148 mmol g^{-1}) for 10 wt% MoO_3/M-ZrPO-700. This indicated the acidic properties were successfully improved by the introduced Mo species which existed as highly dispersed states. However, further increasing the MoO_3 loading to 15 and 20 wt%, the intensity of peak decreased and the acidity decreased to 0.071 and 0.035 mmol·g^{-1}. This might be owing to the aggregation of Mo species, which led to the decrease of acid sites in the materials.

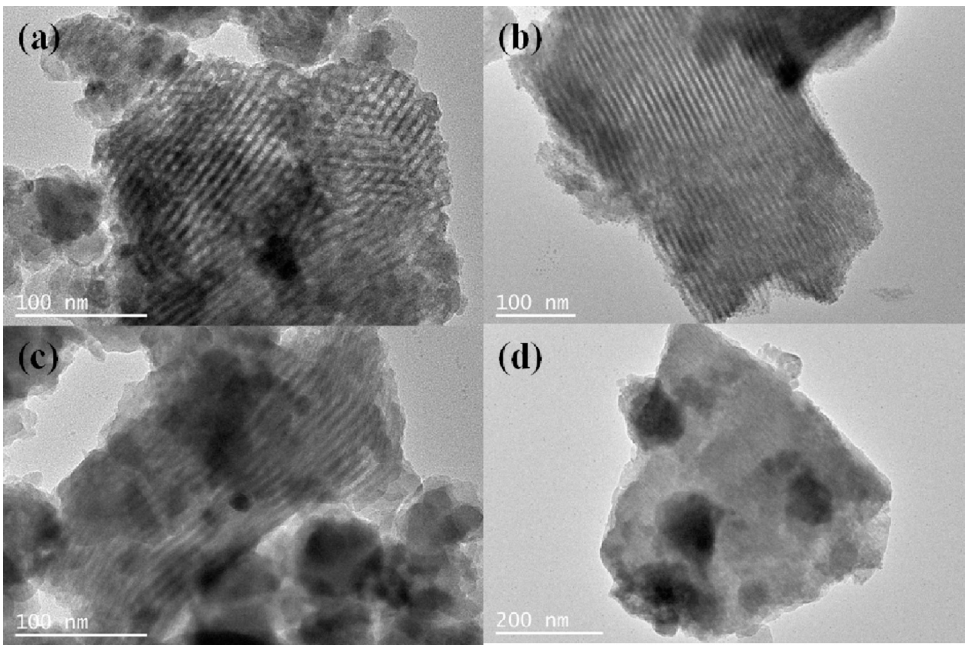

Fig. 6. TEM images of MoO_3/M-ZrPO with differernt MoO_3 loadings treated at 700 °C: **(a)** 5 wt% MoO_3/M-ZrPO, **(b)** 10 wt% MoO_3/M-ZrPO, **(c)** 15 wt% MoO_3/M-ZrPO, **(d)** 20 wt% MoO_3/M-ZrPO.

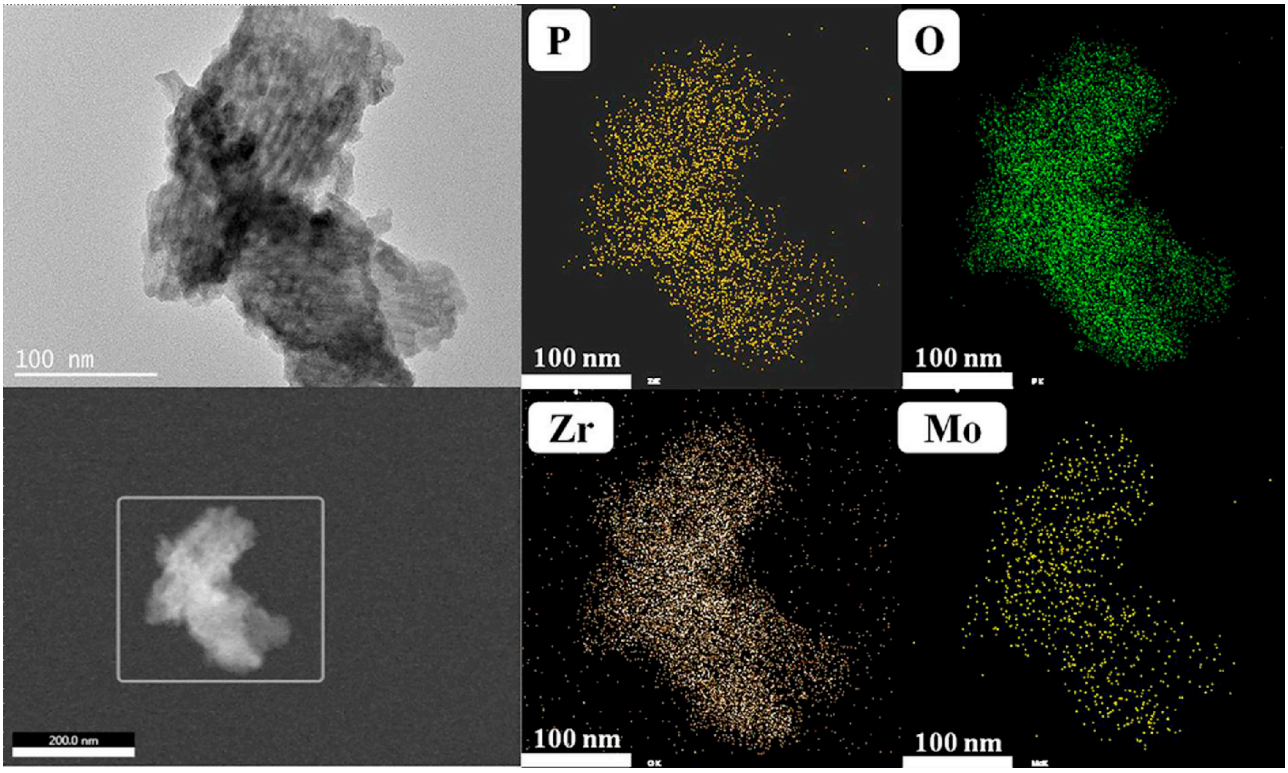

Fig. 7. TEM element mapping of 10 wt% MoO_3/M-ZrPO treated at 700 °C.

The NH_3-TPD patterns of 10 wt% MoO_3/M-ZrPO treated at different calcination temperatures are displayed in Fig. 8(2). The samples calcined under 700 °C exhibited similar pattern, indicating the acidic properties had little change. Nevertheless, the intensity of peak decreased obviously when the calcination temperature reached 800 and 900 °C and the acidity largely decreased to 0.014 and 0.008 mmol·g^{-1}. This might be ascribed to that the highly dispersed Mo species aggregated and formed large MoO_3 particles.

The type of acid sites in the MoO_3/M-ZrPO solid acid catalysts are investigated by the pyridine-IR spectra. As displayed in Fig. 9(1), the bands at 1540 or 1450 cm^{-1}, which were the exclusive bands for Brønsted or Lewis acid sites [36,50,51], could be observed, implying both Brønsted and Lewis acid sites existed in the MoO_3/M-ZrPO solid acid catalysts. In addition, with increasing of MoO_3 loading from 0 to 10 wt%, the intensity of bands, especially for the bands at 1540 cm^{-1}, was gradually improved, indicating the enhancement

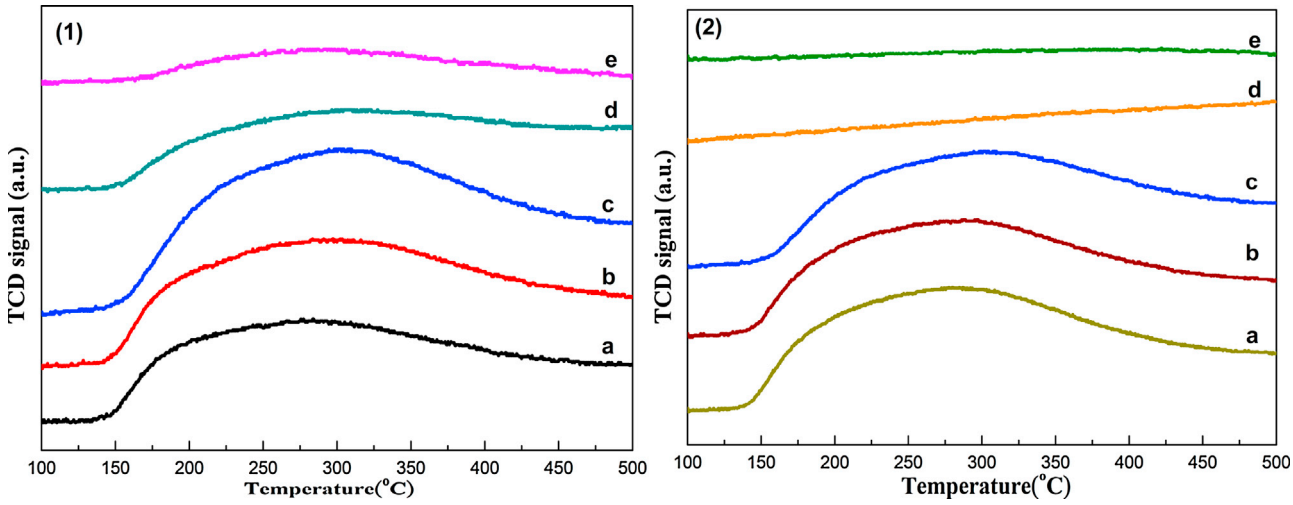

Fig. 8. NH_3-TPD profiles: **(1)** MoO_3/M-ZrPO with differernt MoO_3 loadings treated at 700 °C: **(a)** 0 wt% MoO_3/M-ZrPO, **(b)** 5 wt% MoO_3/M-ZrPO, **(c)** 10 wt% MoO_3/M-ZrPO, **(d)** 15 wt% MoO_3/M-ZrPO, **(e)** 20 wt% MoO_3/M-ZrPO; **(2)** 10 wt% MoO_3/M-ZrPO treated at different temperatures: **(a)** 500 °C, **(b)** 600 °C, **(c)** 700 °C, **(d)** 800 °C, **(e)** 900 °C.

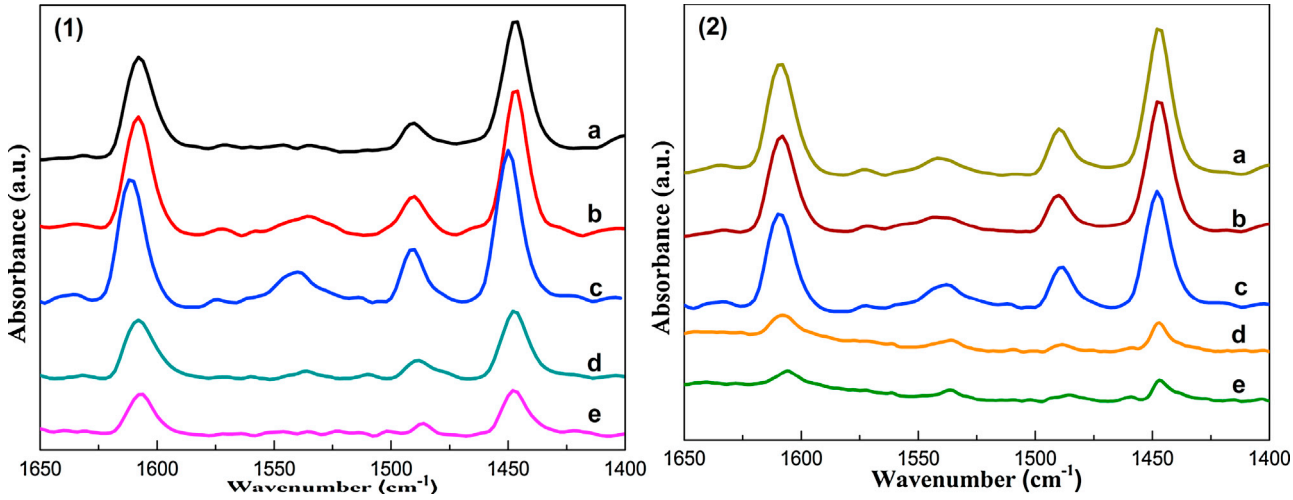

Fig. 9. IR spectra for adsorbed pyridine: **(1)** MoO_3/M-ZrPO with differernt MoO_3 loadings treated at 700 °C: **(a)** 0 wt% MoO_3/M-ZrPO, **(b)** 5 wt% MoO_3/M-ZrPO, **(c)** 10 wt% MoO_3/M-ZrPO, **(d)** 15 wt% MoO_3/M-ZrPO, **(e)** 20 wt% MoO_3/M-ZrPO; **(2)** 10 wt% MoO_3/M-ZrPO treated at different temperatures: **(a)** 500 °C, **(b)** 600 °C, **(c)** 700 °C, **(d)** 800 °C, **(e)** 900 °C.

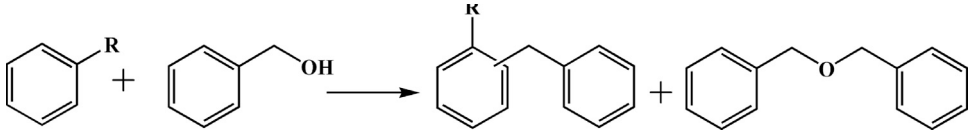

Scheme 1. Friedel-Crafts alkylation reaction between substrates and benzyl alcohol.

of acidic properties by the introduced Mo species. Further increasing the MoO_3 loading to 15 and 20 wt%, the intensity decreased gradually. In addition, as given in Fig. 9(2), the patterns of 10 wt% MoO_3/M-ZrPO solid acid catalysts with calcination temperature under 700 °C had little change, however, the intensity decreased drastically when the temperature reached 800 and 900 °C. This kept consistent with the conclusion gotten from the NH_3-TPD characterization.

3.6. Catalytic performance

The MoO_3/M-ZrPO materials were taken as solid acid catalysts in alkylation reactions (as shown in Scheme 1). In the first set of experiment, alkylation of anisole with benzyl alcohol was performed over MoO_3/M-ZrPO catalysts. In this reaction system, benzylanisoles (BA) was produced as principal product and dibenzyl ether (DBE) is by-product of benzyl alcohol self-etherification [23,25]. The catalytic performance of MoO_3/M-ZrPO solid acid catalysts with various MoO_3 loadings is depicted in Fig. 10(1). Difference in MoO_3 loadings led to a distinct difference in catalytic performance for alkylation reaction. The 0 wt% MoO_3/M-ZrPO, without introduction of Mo species, only exhibited 5.02% conversion of benzyl alcohol and 60.2% selectivity of BA. However, with introduction of MoO_3 species, an obvious improvement in conversion, selectivity and yield was observed and achieved optimal activity at 10 wt% MoO_3/M-ZrPO with 100% conversion of benzyl alcohol and 91.3% selectivity of BA. The gradual enhancement in catalytic performance might be ascribed to the increasing of acid sites, especially

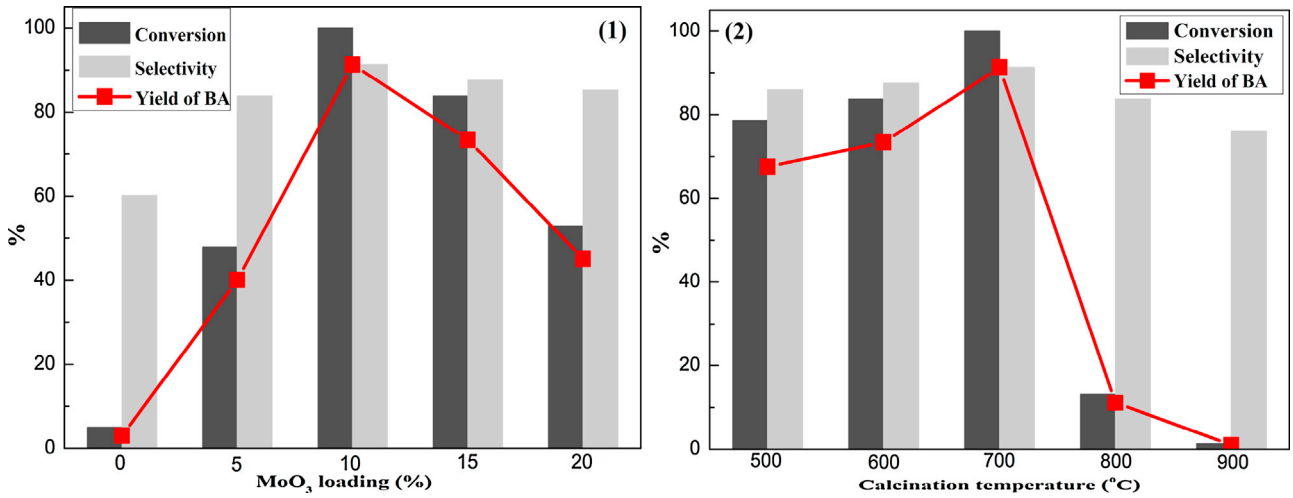

Fig. 10. Friedel-Crafts alkylation reaction between anisole and benzyl alcohol catalyzed by MoO_3/M-ZrPO: **(1)** different MoO_3 loadings and **(2)** different calcination temperatures. (Reaction conditions: anisole 10 mL, benzyl alcohol 1 mL, catalysts 0.1 g, 150 °C, 1 h).

for Brønsted acid sites, which produced by introduction of Mo species in MoO_3/M-ZrPO. However, further increasing MoO_3 loadings to 15 and 20 wt%, the catalytic performance began to decrease. This might be owing to the appearance of crystalline structure and decrease of mesoporous structure, therefore, the amounts of active sites decreased.

The catalytic activity of MoO_3/M-ZrPO with different calcination temperatures (500–900 °C) in alkylation reaction was also researched. As given in Fig. 10(2), slight improvement in conversion and selectivity could be found with calcination temperature increased from 500 to 700 °C. Nevertheless, further increasing calcination temperature to 800 and 900 °C, a "free-fall" decrease in catalytic performance was clearly observed and there only showed conversion 13.2% and 1.21% for 10 wt% MoO_3/M-ZrPO calcined at 800 and 900 °C. As aforementioned characterizations about 10 wt% MoO_3/M-ZrPO materials treated at different temperatures, ordered mesostructure completely vanished and the Mo species in pore wall of mesostructure began to get together and form crystal MoO_3. The recession in specific surface area and aggregation of Mo species might lead to reduction in performance of 10 wt% MoO_3/M-ZrPO after treated at 800 and 900 °C. Based on the above discussion, following conclusion could be made that both high specific surface area and high dispersion of Mo species were beneficial for improvement of catalytic activity. This speculation could also be verified by

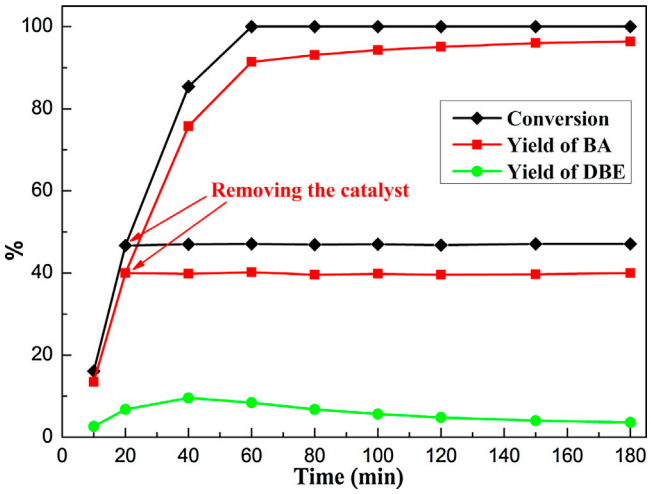

Fig. 11. Friedel-Crafts alkylation reaction catalyzed by 10 wt% MoO_3/M-ZrPO at different times. (Reaction conditions: anisole 10 mL, benzyl alcohol 1 mL, catalysts 0.1 g, 150 °C).

X wt% MoO_3/M-ZrPO treated at 600 °C. As shown in Fig. S4, catalytic performance of catalysts was gradually improved from 0 to 15 wt%

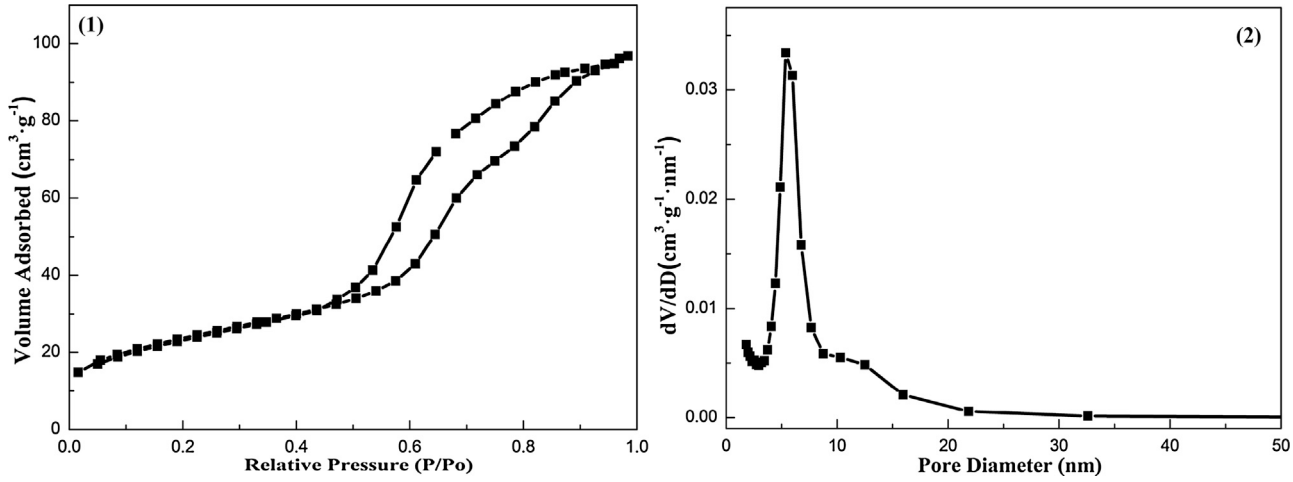

Fig. 12. Isotherm **(1)** and pore size distributions **(2)** of used 10 wt% MoO_3/M-ZrPO catalyst.

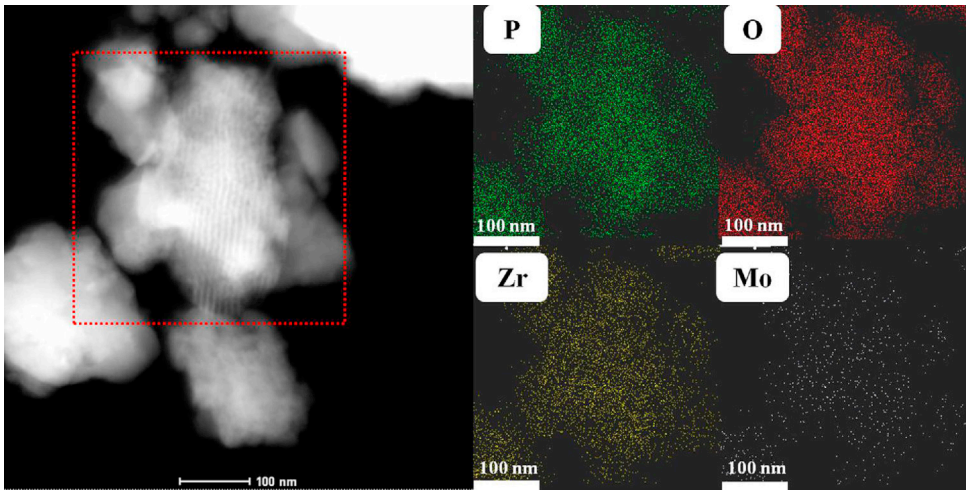

Fig. 13. TEM element mapping of used 10 wt% MoO_3/M-ZrPO catalyst.

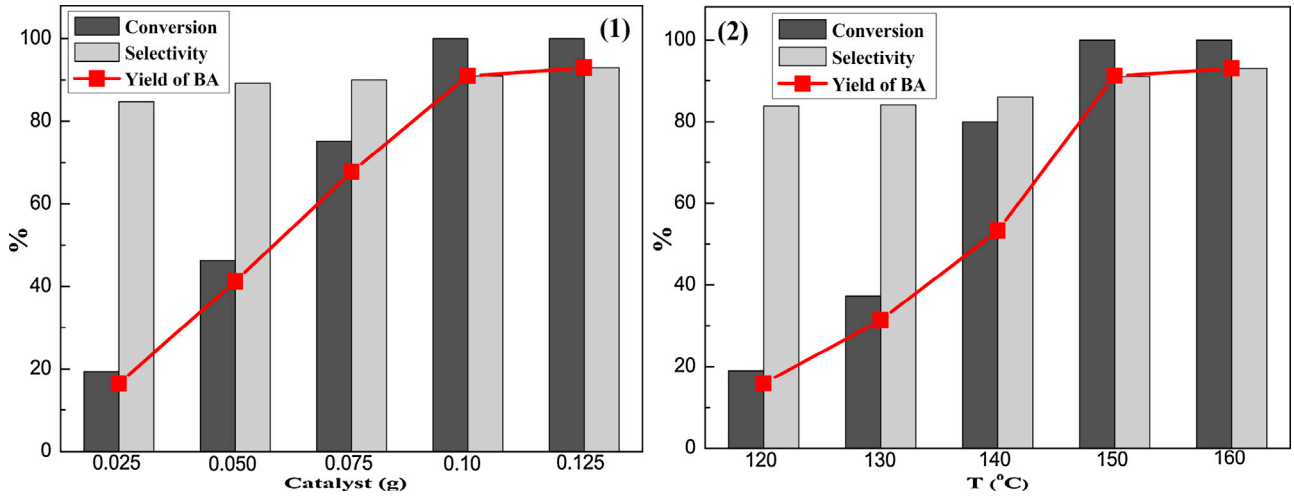

Fig. 14. Friedel-Crafts alkylation reaction catalyzed by MoO_3/M-ZrPO: **(1)** different amount of catalyst; **(2)** different reaction temperature. (Reaction conditions: anisole 10 mL, benzyl alcohol 1 mL, 1 h).

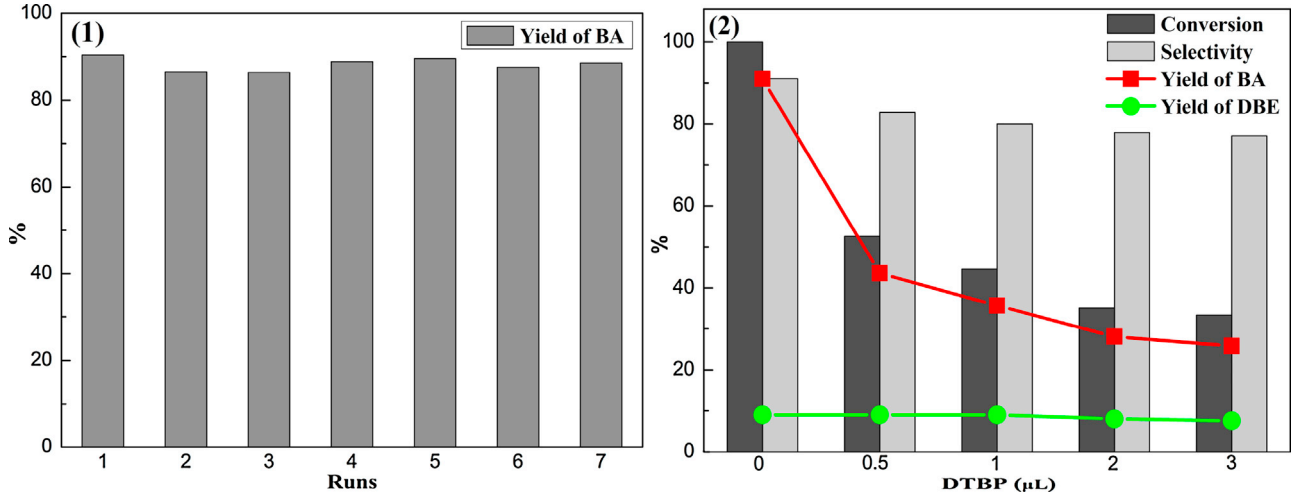

Fig. 15. Friedel-Crafts alkylation reaction catalyzed by MoO_3/M-ZrPO: **(1)** reused for seven cycles; **(2)** poisoned by 2,6-DTBP. (Reaction conditions: anisole 10 mL, benzyl alcohol 1 mL, catalysts 0.1 g, 150 °C, 1 h).

with Mo species existed as highly dispersed states. Compared with this, the activity of catalyst began to reduce for 20 wt% MoO_3/M-ZrPO and 25 wt% MoO_3/M-ZrPO, which had crystalline structure and poor mesoporous properties.

Table 2
Alkylation of different arenes and alkylating agents over 10 wt% MoO_3/M-ZrPO-700 .

Entry	Arenes	Alkylating agents	Alkylation products	Con. (%)	Sel. (%)[d]
1[a]		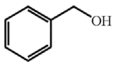	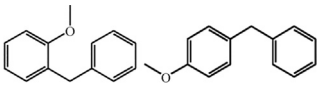	100	41:50
2[a]		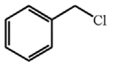	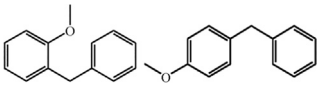	99.1	42:58
3[a]		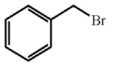	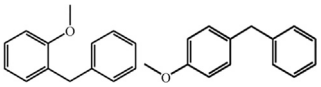	82.0	43:57
4[a]		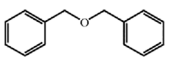	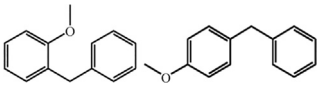	97.3	49:51
5[a]		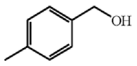	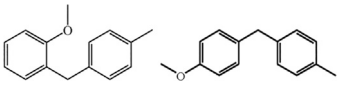	100	36:64
6[b]		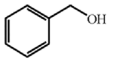	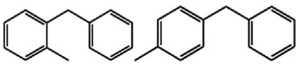	75.2	33:28
7[c]		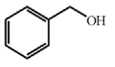	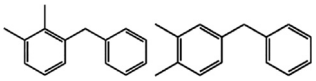	99.6	69:28
8[c]		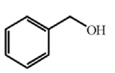	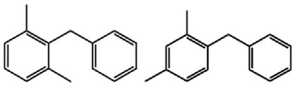	100	18:82
9[c]		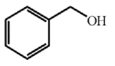	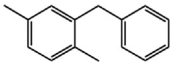	86.7	57
10[c]		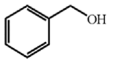	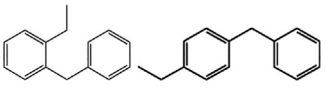	90.2	37:25
11[c]		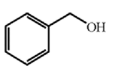	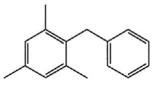	100	100
12[c]	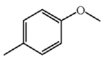	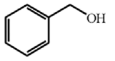	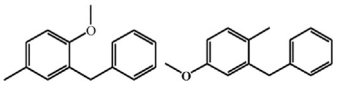	100	74:18

Reaction conditions.
[a] arene: 0.10 mol, alkylation agent: 0.01 mol, catalyst: 0.1 g, 150 °C, 1 h.
[b] arene: 0.10 mol, alkylation agent: 0.005 mol, catalyst: 0.1 g, 110 °C, 2 h.
[c] arene: 0.10 mol, alkylation agent: 0.005 mol, catalyst: 0.1 g, 150 °C, 2 h.
[d] The by-product was dibenzyl ether (DBE) in these reactions.

The progress of alkylation and heterogeneity of 10 wt% MoO_3/M-ZrPO was determined by researching products at different intervals. As shown in Fig. 11, conversion of benzyl alcohol increased with time from 0 to 60 min and gotten 100% at 60 min for 10 wt% MoO_3/M-ZrPO. Furthermore, as an excellent solid acid catalyst, heterogeneity was very important, and the leaching test should be investigated. As displayed in Fig. 11, the 10 wt% MoO_3/M-ZrPO catalysts were removed at 20 min from the reaction system. After that, few variations were observed in conversion of benzyl alcohol and yield of BA, indicating that 10 wt% MoO_3/M-ZrPO was a truly heterogeneous catalyst and no obvious active components were leached into liquid phase in the progress of alkylation.

Furthermore, the used catalyst was researched by N_2-physisorption and TEM techniques to study stability of 10 wt% MoO_3/M-ZrPO. As shown in Fig. 12, H1 typed hysteresis loops and intensive pore size distribution still maintained in the used 10 wt% MoO_3/M-ZrPO. Meanwhile, specific surface area (72 $m^2\ g^{-1}$), pore size (7.08 nm) and pore volume (0.13 $cm^3\ g^{-1}$) had little change, implying that 10 wt% MoO_3/M-ZrPO catalyst suffered little change in process of acid-catalyzed reaction. Moreover, as given in Fig. 13, ordered mesoporous structure with highly dispersed Mo species still maintained in used catalyst. Meanwhile, Mo content of used catalyst was investigated by XRF characterization. Compared with fresh catalyst (10.1 wt%), MoO_3 loadings (10.3 wt%) of used catalyst changed little, indicating the excellent stability of catalysts and no obvious Mo species were leached into liquid phase in process of reaction.

In this section, details on influence of catalyst amounts and reaction temperatures on FC alkylation reaction were researched and the results are given in Fig. 14. It could be clearly observed that conversion of benzyl alcohol, selectivity and yield of BA were improved gradually with enhancing of catalyst amounts from 0.025 to 0.1 g. The 100% conversion and 91.3% selectivity were achieved when amount of catalyst reached 0.1 g. Therefore, the presence of

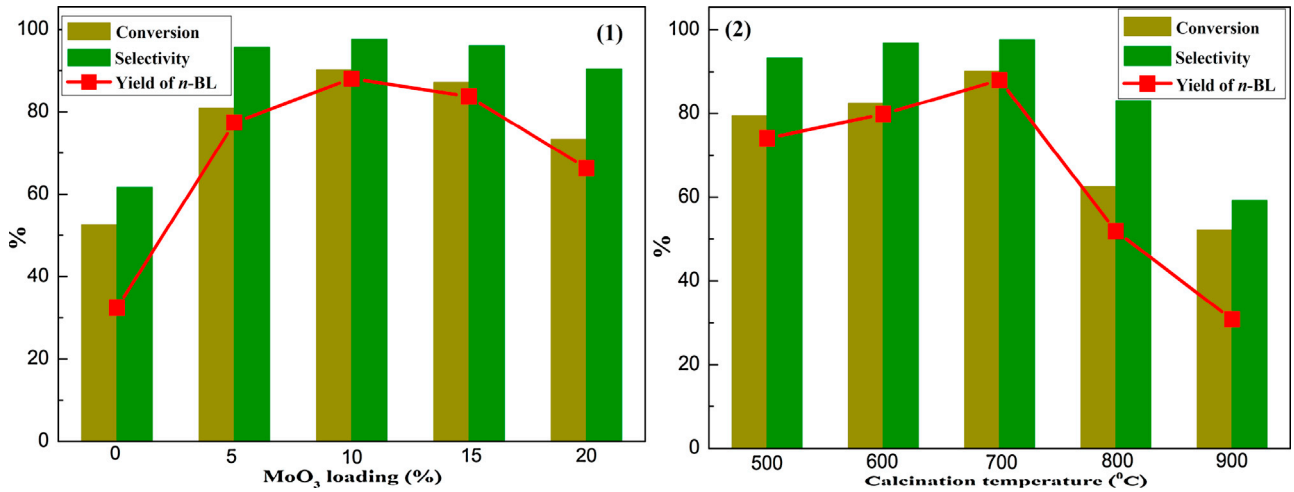

Fig. 16. Esterification of levulinic acid with 1-butanol catalyzed by MoO_3/M-ZrPO: **(1)** different MoO_3 loadings and **(2)** different calcination temperatures. (Reaction conditions: 1-butanol 10 mL, levulinic acid 1 mL, catalysts 0.1 g, 120 °C, 4 h).

adequate acid sites was in favor of improving the catalytic performance. Further increasing catalyst amount to 0.125 g, catalytic activity changed little. Moreover, conversion of benzyl alcohol and selectivity of BA gradually enhanced with increasing of reaction temperatures and reached maximum at 150 °C.

For sake of checking the reutilization of catalyst, a seven runs test over 10 wt% MoO_3/M-ZrPO-700 was carried out under aforementioned reaction conditions (shown in Fig. 15(1)). It was noteworthy that no significant declines in catalytic performance were observed and the yield of BA could reach 90% even after seven cycles compared with fresh catalyst, indicating that 10 wt% MoO_3/M-ZrPO-700 had excellent reusability and could be reused as solid acid catalyst. It might be owing to excellent stability of catalysts and no active sites were leached into liquid phase in process of reaction.

To further investigate influence of acid sites in FC alkylation, catalytic activity of 10 wt% MoO_3/M-ZrPO poisoned by different amounts of 2,6-Di-tert-butylpyridine (2,6-DTBP), which was thought to mainly adsorb on the accessible Brønsted acid sites in solid acid catalysts [52–55], have been studied. As shown in Fig. 15(2), with addition of 2,6-DTBP increasing from 0 to 3 μL, conversion of benzyl alcohol and yield of BA gradually decreased. This indicated that FC alkylation of anisole with benzyl alcohol mainly reacted on the Brønsted acid sites in 10 wt% MoO_3/M-ZrPO. Moreover, yield of DBE changed little with addition of 2,6-DTBP and this might be owing to that auto-etherification of benzyl alcohol mainly happened on the Lewis acid sites of MoO_3/M-ZrPO.

The alkylation of different arenes (methylbenzene, *ortho*-xylene, *meta*-xylene, *para*-xylene, ethylbenzene, mesitylene, 4-methylanisole) and alkylating agents (benzyl chloride, benzyl bromide and dibenzyl ether) over 10 wt% MoO_3/M-ZrPO is shown in Table 2. It was noteworthy to mention that 10 wt% MoO_3/M-ZrPO exhibited excellent catalytic performance for alkylation with different arenes and alkylating agents. This indicated that 10 wt% MoO_3/M-ZrPO was an excellent solid acid catalyst for alkylation reaction.

Moreover, MoO_3/M-ZrPO solid acid was employed in esterification of levulinic acid (LA) with 1-butanol (1-BuOH) (as shown in Scheme 2). As shown in Fig. 16, the catalytic activity (conversion of LA, selectivity and yield of *n*-BL) of MoO_3/M-ZrPO solid acid was improved with enhancement of MoO_3 loadings and calcination temperature and 10 wt% MoO_3/M-ZrPO solid acid catalyst treated at 700 °C exhibited optimal catalytic performance (90.2% conversion of LA and 97.6% selectivity of *n*-BL). Further increasing MoO_3 loadings to 15 and 20 wt%, calcination temperature to 800 and 900 °C, catalytic performance began to decrease. This further confirmed the above conclusion. The influence of reaction times, catalyst amounts and reaction temperatures on esterification is displayed in Fig. S5 and S6 . The catalytic performance was gradually improved and gotten 90.2% conversion of LA and 97.6% selectivity of *n*-BL when the reaction time, catalyst amount and reaction temperature reached 4 h, 0.1 g and 120 °C.

4. Conclusion

In this paper, a novel MoO_3/M-ZrPO solid acid catalysts with different MoO_3 loadings (0–20 wt%) and different calcination temperatures (500–900 °C) have been synthesized and employed in Friedel-Crafts alkylation and esterification. All the results indicated that the highly dispersed polymolybdate species and excellent mesostructure were in favor of improving the catalytic performance of catalysts. In addition, MoO_3/M-ZrPO catalysts showed excellent catalytic performance in Friedel-Crafts alkylation of different aromatic compounds and esterification of levulinic acid with 1-butanol. Moreover, it was noteworthy that the catalyst had superior reusability and there were no obvious declines in catalytic performance even after seven runs. Therefore, MoO_3/M-ZrPO was a promise and environmentally benign solid acid catalyst.

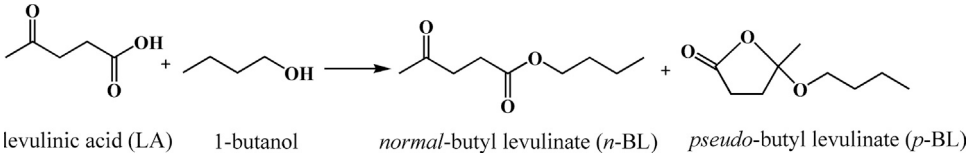

Scheme 2. Esterification of levulinic acid with 1-butanol.

Acknowledgements

The authors sincerely acknowledge the financial support from the Natural Science Foundation of China (21576158 and 21576159), Shandong Provincial Natural Science Foundation (2015ZRB0176).

Appendix A. Supplementary data

Supplementary data associated with this article can be found, in the online version, at http://dx.doi.org/10.1016/j.mcat.2017.10.028.

References

[1] J.W. Harris, M.J. Cordon, J.R. Di Iorio, J.C. Vega-Vila, F.H. Ribeiro, R. Gounder, J. Catal. 335 (2016) 141–154.
[2] M. Haneda, K. Takamura, Y. Doi, N. Bion, L. Vivier, J. Mater. Sci. 52 (2017) 5835–5845.
[3] E. Wada, M. Kitano, K. Yamamoto, K. Nakajima, S. Hayashi, M. Hara, Catal. Sci. Technol. 6 (2016) 4832–4839.
[4] Z. Wang, L. Wang, Y. Jiang, M. Hunger, J. Huang, ACS Catal. 4 (2014) 1144–1147.
[5] Z. Buniazet, J. Couble, D. Bianchi, M. Rivallan, A. Cabiac, S. Maury, S. Loridant, J. Catal. 348 (2017) 125–134.
[6] Y. Li, D. Zeng, Mater. Lett. 193 (2017) 172–175.
[7] A. Corma, H. García, Chem. Rev. 102 (2002) 3837–3892.
[8] G. Busca, Chem. Rev. 107 (2007) 5366–5410.
[9] T. Okuhara, Chem. Rev. 102 (2002) 3641–3666.
[10] I.M. Lokman, U. Rashid, R. Yunus, Y.H. Taufiq-Yap, Cat. Rev. Sci. Eng. 56 (2014) 187–219.
[11] E. Rossmedgaarden, W. Knowles, T. Kim, M. Wong, W. Zhou, C. Kiely, I. Wachs, J. Catal. 256 (2008) 108–125.
[12] P. Wang, J. Feng, Y. Zhao, S. Wang, J. Liu, ACS Appl. Mater. Interfaces 8 (2016) 23755–23762.
[13] L. Li, Y. Yoshinaga, T. Okuhara, Phys. Chem. Chem. Phys. 4 (2002) 6129–6136.
[14] N. Lamine, A. Benadda, A. Djadoun, A. Barama, J. Blanchard, J. Mol. Catal. A: Chem. 425 (2016) 157–165.
[15] B. Madje, P. Patil, S. Shindalkar, S. Benjamin, M. Shingare, M. Dongare, Catal. Commun. 5 (2004) 353–357.
[16] J. Xu, A. Zheng, J. Yang, Y. Su, J. Wang, D. Zeng, M. Zhang, C. Ye, F. Deng, J. Phys. Chem. B 110 (2006) 10662–10671.
[17] A. Martínez, G. Prieto, M.A. Arribas, P. Concepción, J.F. Sánchez-Royo, J. Catal. 248 (2007) 288–302.
[18] S. Li, H. Zhou, C. Jin, N. Feng, F. Liu, F. Deng, J.-Q. Wang, W. Huang, L. Xiao, J. Fan, J. Phys. Chem. C 118 (2014) 6283–6290.
[19] T. Yamamoto, A. Teramachi, A. Orita, A. Kurimoto, T. Motoi, T. Tanaka, J. Phys. Chem. C 120 (2016) 19705–19713.
[20] D. Yin, C. Li, L. Tao, N. Yu, S. Hu, D. Yin, J. Mol. Catal. A: Chem. 245 (2006) 260–265.
[21] M.M. Khodaei, E. Nazari, Tetrahedron Lett. 53 (2012) 5131–5135.
[22] J. Dou, H.C. Zeng, J. Phys. Chem. C 116 (2012) 7767–7775.
[23] A. Ramanathan, H. Zhu, R. Maheswari, B. Subramaniam, J. Chem. Eng. 278 (2015) 113–121.
[24] C. Ramesh Kumar, S.M, N. Lingaiah, Appl Catal. A 487 (2014) 165–171.
[25] M.J. Gracia, E. Losada, R. Luque, J.M. Campelo, D. Luna, J.M. Marinas, A.A. Romero, Appl. Catal. A 349 (2008) 148–155.
[26] J.H. Clark, Green Chem. 1 (1999) 1–8.
[27] X. Liang, J. Chem Eng, (2015) 251–257.
[28] M. Lee, Y. Seo, H.S. Shin, C. Jo, R. Ryoo, Microporous Mesoporous Mater. 222 (2016) 185–191.
[29] T. Yutthalekha, C. Wattanakit, C. Warakulwit, W. Wannapakdee, K. Rodponthukwaji, T. Witoon, J. Limtrakul, J. Clean Prod. 142 (2017) 1244–1251.
[30] A. Nagaraj, D. Amarajothi, J. Colloid Interface Sci. 494 (2017) 282–289.
[31] K. Saravanan, B. Tyagi, R.S. Shukla, H.C. Bajaj, Fuel 165 (2016) 298–305.
[32] M.A. Tejero, E. Ramírez, C. Fité, J. Tejero, F. Cunill, Appl. Catal. A 517 (2016) 56–66.
[33] Y.H. Chung, T.H. Peng, H.Y. Lee, C.L. Chen, I.L. Chien, Ind. Eng. Chem. Res. 54 (2015) 3341–3354.
[34] D. Song, S. An, Y. Sun, Y. Guo, J. Catal. 333 (2016) 184–199.
[35] X. Zhou, Z.X. Li, C. Zhang, X.P. Gao, Y.Z. Dai, G.Y. Wang, J. Mol. Catal. A: Chem. 417 (2016) 71–75.
[36] S.S. Enumula, V.R.B. Gurram, R.R. Chada, D.R. Burri, S.R.R. Kamaraju, J. Mol. Catal. A: Chem. 426 (2017) 30–38.
[37] W. Ciptonugroho, M.G. Al-Shaal, J.B. Mensah, R. Palkovits, J. Catal. 340 (2016) 17–29.
[38] M. Wu, X. Zhang, X. Su, X. Li, X. Zheng, X. Guan, P. Liu, Catal. Commun. 85 (2016) 66–69.
[39] J. Čejka, S. Mintova, Catal. Rev. Sci. Eng. 49 (2007) 457–509.
[40] Y. Ren, Z. Ma, P.G. Bruce, Chem. Soc. Rev. 41 (2012) 4909–4927.
[41] S. Rostamnia, N. Nouruzi, H. Xin, R. Luque, Catal. Sci. Technol. 5 (2015) 199–205.
[42] E. Doustkhah, S. Rostamnia, H.G. Hossieni, R. Luque, ChemistrySelect 2 (2017) 329–334.
[43] D. Gu, F. Schüth, Chem. Soc. Rev. 43 (2014) 313–344.
[44] S. Rostamnia, E. Doustkhah, B. Zeynizadeh, Microporous Mesoporous Mater. 222 (2016) 87–93.
[45] S. Rostamnia, S. Kholdi, J. Phys. Chem. Solids 111 (2017) 47–53.
[46] Z. Miao, L. Xu, H. Song, H. Zhao, L. Chou, Catal. Sci. Technol. 3 (2013) 1942–1954.
[47] A. Calafat, L. Avilán, J. Aldana, Appl. Catal. A 201 (2000) 215–223.
[48] T. Bhaskar, K.R. Reddy, C.P. Kumar, M.R.V.S. Murthy, K.V.R. Chary, Appl. Catal. A 211 (2001) 189–201.
[49] Y. Cui, N. Liu, Y. Xia, J. Lv, S. Zheng, N. Xue, L. Peng, X. Guo, W. Ding, J. Mol. Catal. A: Chem. 394 (2014) 1–9.
[50] A.M. Alsalme, P.V. Wiper, Y.Z. Khimyak, E.F. Kozhevnikova, I.V. Kozhevnikov, J. Catal. 276 (2010) 181–189.
[51] L. Brahmi, T. Ali-Dahmane, R. Hamacha, S. Hacini, J. Mol. Catal. A: Chem. 423 (2016) 31–40.
[52] A. Corma, V. Fornés, L. Forni, F. Márquez, J. Martıínez-Triguero, D. Moscotti, J. Catal. 179 (1998) 451–458.
[53] J. Wang, W. Hua, Y. Yue, Z. Gao, Bioresour. Technol. 101 (2010) 7224–7230.
[54] K. Góra-Marek, K. Tarach, M. Choi, J. Phys. Chem. C 118 (2014) 12266–12274.
[55] L. Emdadi, S.C. Oh, Y. Wu, S.N. Oliaee, Y. Diao, G. Zhu, D. Liu, J. Catal. 335 (2016) 165–174.